J. Fluid Mech. (2001), *vol.* 445, *pp.* 55–76.
DOI: 10.1017/S0022112001005274 Printed in the United Kingdom

A correlation for the lift-off of many particles in plane Poiseuille flows of Newtonian fluids

By N. A. PATANKAR[1]†, T. KO[1], H. G. CHOI[2] AND D. D. JOSEPH[1]

[1]Department of Aerospace Engineering and Mechanics and the Minnesota Supercomputer Institute, University of Minnesota, Minneapolis, MN 55455, USA

[2]School of Mechanical and Aerospace Engineering, Seoul National University, Seoul 151-742, South Korea

(Received 27 September 2000 and in revised form 27 February 2001)

Choi & Joseph (2001) reported a two-dimensional numerical investigation of the lift-off of 300 circular particles in plane Poiseuille flows of Newtonian fluids. We perform similar simulations. Particles heavier than the fluid are initially placed in a closely packed ordered configuration at the bottom of a periodic channel. The fluid–particle mixture is driven by an external pressure gradient. The particles are suspended or fluidized by lift forces that balance the buoyant weight perpendicular to the flow. Pressure waves corresponding to the waves at the fluid–mixture interface are observed. During the initial transient, these waves grow, resulting in bed erosion. At sufficiently large shear Reynolds numbers the particles occupy the entire channel width during the transient. The particle bed eventually settles to an equilibrium height which increases as the shear Reynolds number is increased. Heavier particles are lifted to a smaller equilibrium height at the same Reynolds number. A correlation for the lift-off of many particles is obtained from the numerical data. The correlation is used to estimate the critical shear Reynolds number for lift-off of many particles. The critical shear Reynolds number for lift-off of a single particle is found to be greater than that for many particles. The procedures used here to obtain correlations from direct simulations in two dimensions and the type of correlations that emerge should generalize to three-dimensional simulations at present underway.

1. Introduction

Lift plays a central role in the suspension of particles in the flow of slurries. In the oil industry we can consider the removal of drill cuttings in horizontal drill holes and sand (or proppant) transport in fractured reservoirs. A force experienced by a particle moving through a fluid with circulation (or shearing motion for a viscous fluid) is referred to as the lift force in the present work.

Modelling of solid–liquid mixtures has been approached in two ways. The first approach is to consider the solid–liquid mixture as an effective fluid medium. Bulk properties (such as the effective viscosity) of the composite mixture are then modelled. In the second approach the solid and the fluid are considered as inter-penetrating mixtures which are governed by conservation laws. Interaction between the inter-penetrating phases is modelled. This is the mixture theory approach. Models for drag

† Current address: Department of Mechanical Engineering, Northwestern University, Evanston, IL 60208, USA.

and lift forces on the particles must be used in mixture theories. Models for the drag force on particles in solid–liquid mixtures are a complicated issue and usually rely on the well-known Richardson–Zaki (1954) correlation. Models for lift forces in mixtures are much less well developed than models for drag.

Joseph (2001) proposed that ideas analogous to the Richardson–Zaki correlation must come into play in problems of slurries, which are fluidized by lift rather than by drag. Various models for the lift on single particles have been proposed (see e.g. Joseph 2001; Patankar *et al.* 2001; Ko, Patankar & Joseph 2001 and references therein) but the dependence of the lift on solids fraction and other many particle parameters is not known. Direct numerical simulations or experiments can be done to develop a suitable engineering correlation for lift.

Morris & Brady (1998) studied the migration of non-neutrally buoyant spheres in pressure-driven flows of Newtonian fluids. They performed Stokesian dynamic simulations of a monolayer of spheres. These studies are valid in the creeping flow limit. In applications such as the transport of slurries or proppants, the effect of Reynolds number on the lift force is important. Choi & Joseph (2001, hereafter referred to as CJ) reported a two-dimensional numerical investigation of fluidization by lift of 300 circular particles in a Poiseuille flow of a Newtonian fluid. Their results are valid at finite shear Reynolds numbers. They observed that the fluidization of circular particles first involves bed inflation in which liquid is driven into the bed. The bed inflation was observed even at very low shear Reynolds numbers but it took more time for the bed to inflate as the Reynolds number was reduced. Pressure waves corresponding to the waves at the fluid–mixture interface were observed. CJ used a Chorin (1968) type fractional-step scheme developed by Choi (2000) to perform the numerical simulations. We use the same numerical method for the simulations reported in this paper. This method is closely related to the arbitrary-Lagrangian–Eulerian (ALE) numerical method, using body-fitted unstructured finite element grids to simulate particulate flows, reported by Hu, Joseph & Crochet (1992), Hu (1996), Hu & Patankar (2001) and Hu, Patankar & Zhu (2001). In these simulations the distance between the particles cannot be equal to zero. We have a small zone around each particle, which we call the security zone. Overlap of the security zones gives rise to a repulsive force that keeps the particles apart.

In this paper an engineering type correlation for the lift-off of many particles is obtained using the numerical data from our simulations and from the simulations of CJ. We also study the effect of various parameters on the flow features. Both the transient and the steady-state behaviour will be discussed.

The governing equations, various parameters of the problem and a discussion of the lift models for solid–liquid flows will be presented in § 2. Results will be presented in § 3 and conclusions in § 4.

2. Governing equations and the parameters of the problem

The two-dimensional computational domain for our simulations is shown in figure 1. We perform simulations in a periodic domain (figure 2). The applied pressure gradient is given by $-\bar{p}$, where $\bar{p}$ is considered to be positive. We split the pressure as follows:

$$\begin{aligned} P &= p + \rho_f \boldsymbol{g} \cdot \boldsymbol{x} - \bar{p}\boldsymbol{e}_x \cdot \boldsymbol{x} \\ \Rightarrow -\nabla P &= -\nabla p - \rho_f \boldsymbol{g} + \bar{p}\boldsymbol{e}_x, \end{aligned} \tag{1}$$

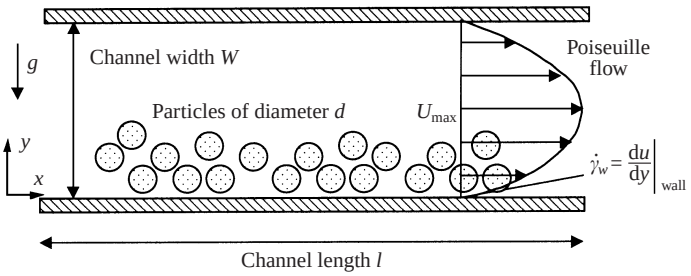

FIGURE 1. Computational domain for the numerical simulation of lift-off of particles in a plane Poiseuille flow. The wall shear rate $\dot{\gamma}_w$ is calculated from the parabolic velocity profile in the absence of the particles.

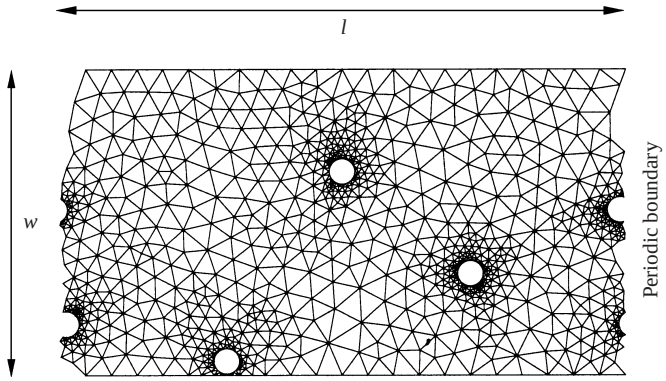

FIGURE 2. Unstructured mesh in a periodic domain.

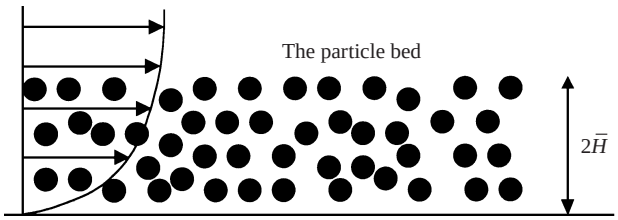

FIGURE 3. Particles fluidized in a Poiseuille flow.

where $P(\boldsymbol{x}, t)$ is the total fluid pressure, ρ_f is the fluid density, $\boldsymbol{g}$ is the acceleration due to gravity, $\boldsymbol{x}$ is the position vector and $\boldsymbol{e_x}$ is the unit vector in the x-direction. We solve for the 'dynamic' pressure p in our simulations. The external pressure gradient term then appears as a body-force-like term in the fluid and particle equations (3). The value of $\bar{p}$ is specified during the simulations.

The particles are free to rotate and translate. Particles heavier than the fluid are initially placed in a closely packed ordered configuration at the bottom of the channel. Gravity acts in the negative y-direction. A parabolic velocity profile corresponding to $\bar{p}$ is specified in the clear fluid region as the initial condition. This reduces the time of the initial transient significantly. At $t = 0_+$ the fluid in the channel is driven by an external pressure gradient along the x-direction. The particles are suspended or fluidized by lift forces that balance the buoyant weight perpendicular to the flow (figure 3).

The average height $\bar{H}$ of the particle bed reaches an equilibrium value after the initial transient. We define this state as the 'statistical steady state'. The average height represents the height of the centre of gravity of the bed if the distribution of the particles in the bed is uniform. The average fluid fraction ϵ of the bed is given by

$$\epsilon = 1 - \frac{N\pi d^2}{8\bar{H}l}, \tag{2}$$

where N is the number of particles in the domain and d is the diameter of the particles.

The governing equations in non-dimensional form are

$$\left.\begin{aligned} &\nabla \cdot \boldsymbol{u} = 0, \\ &R\left(\frac{\partial \boldsymbol{u}}{\partial t} + (\boldsymbol{u}\cdot\nabla)\boldsymbol{u}\right) = -\nabla p + 2\frac{d}{W}\boldsymbol{e_x} + \nabla\cdot\boldsymbol{T}, \\ &\boldsymbol{T} = \boldsymbol{A}, \end{aligned}\right\} \text{fluid} \tag{3}$$

$$\left.\begin{aligned} &\frac{\rho_p}{\rho_f}R\frac{\mathrm{d}\boldsymbol{U}_p}{\mathrm{d}t} = 2\frac{d}{W}\boldsymbol{e_x} - \frac{R_G}{R}\boldsymbol{e_y} + \frac{4}{\pi}\oint[-p\boldsymbol{I} + \boldsymbol{T}]\cdot\boldsymbol{n}\mathrm{d}\Gamma, \\ &\frac{\rho_p}{\rho_f}R\frac{\mathrm{d}\boldsymbol{\Omega}_p}{\mathrm{d}t} = \frac{32}{\pi}\oint(\boldsymbol{x}-\boldsymbol{X})\times([-p\boldsymbol{I} + \boldsymbol{T}]\cdot\boldsymbol{n})\mathrm{d}\Gamma, \end{aligned}\right\} \text{particles} \tag{4}$$

where $\boldsymbol{u}(\boldsymbol{x}, t)$ is the fluid velocity, ρ_p is the particle density, $\boldsymbol{T}$ is the extra-stress tensor, $\boldsymbol{A} = (\nabla\boldsymbol{u} + \nabla\boldsymbol{u}^T)$ is two times the deformation-rate tensor, $\boldsymbol{U}_p$ is the translational velocity of the particle, $\boldsymbol{\Omega}_p$ is the angular velocity of the particle, $\boldsymbol{I}$ is the particle moment of inertia tensor, $\boldsymbol{X}$ is the coordinate of the centre of mass of the particle and $\boldsymbol{e_y}$ is the unit vector in the y-direction. We have used $\boldsymbol{g} = -g\boldsymbol{e_y}$. Equations (3) and (4) and the corresponding initial and boundary conditions define an initial boundary value problem that can be solved by direct numerical simulation, The parameters in this problem are

average fluid fraction in the particle bed	ϵ,
number of particles per unit dimensionless length	Nd/l,
shear Reynolds number	$R = \dfrac{\rho_f V d}{\eta} = \dfrac{\rho_f \dot{\gamma}_w d^2}{\eta} = \dfrac{\rho_f W d^2}{2\eta^2}\bar{p}$,
gravity Reynolds number,	$R_G = \dfrac{\rho_f V_g d}{\eta} = \dfrac{\rho_f(\rho_p - \rho_f)g d^3}{\eta^2} = \dfrac{4\rho_f L d}{\pi\eta^2}$,
aspect ratio,	$\dfrac{\bar{p}d^2}{\eta V} = \dfrac{\bar{p}d}{\eta\dot{\gamma}_w} = 2\dfrac{d}{W}$,
density ratio,	$\dfrac{\rho_p}{\rho_f}$,

where $V_g = (\rho_p - \rho_f)gd^2/\eta$ is the velocity scale of a particle sedimenting in a viscous fluid and L is the buoyant weight (or lift) on a particle in the absence of any other particles. The dimensionless channel length l/d, which is also a parameter of the problem, is chosen large enough so that the solution is only weakly dependent on

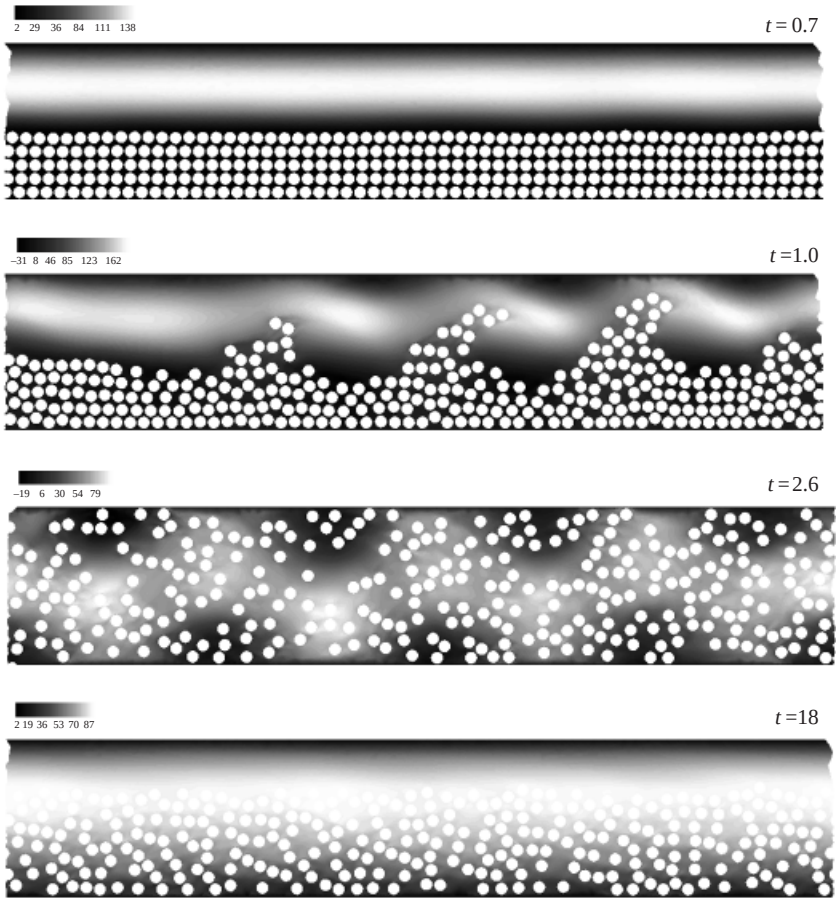

FIGURE 4. Lift-off of 300 heavy particles in a plane Poiseuille flow of a Newtonian fluid; $R = 1800$, $R_G = 981$ and the variables are in CGS units. A contour plot of the horizontal velocity component is shown. Lighter shades indicate higher velocity.

its value. A dimensionless description of the governing equations is constructed by introducing the following scales: the particle diameter d for length, V for velocity, d/V for time, $\eta V/d$ for stress and pressure and V/d for angular velocity of the particle where η is the viscosity of the fluid. We have chosen $V = \dot{\gamma}_w d$, where $\dot{\gamma}_w$ is the shear rate at the wall (in the absence of the particles) corresponding to the applied pressure gradient $\bar{p}$ as shown in figure 1. In our multi-particle simulations we have $N = 300$, $\rho_p/\rho_f = 1.01$, $W/d = 12$ and $l/d = 63$. We take $d = 1\,\mathrm{cm}$, $\rho_p = 1.01\,\mathrm{g\,cm^{-3}}$ and $\rho_f = 1\,\mathrm{g\,cm^{-3}}$.

A gravity parameter G, which represents the ratio of V_g and V, is given by R_G/R. The ratio $R/G = d\dot{\gamma}_w^2/((\rho_p/\rho_f - 1)g)$, which measures the ratio of inertia to buoyant weight, is a generalized Froude number.

Assuming the channel to be long, the gravity Reynolds number at the 'statistical steady state' depends on the parameters listed above and

$$R_G = f\left(R, \epsilon, \frac{Nd}{l}, \frac{W}{d}\right). \tag{5}$$

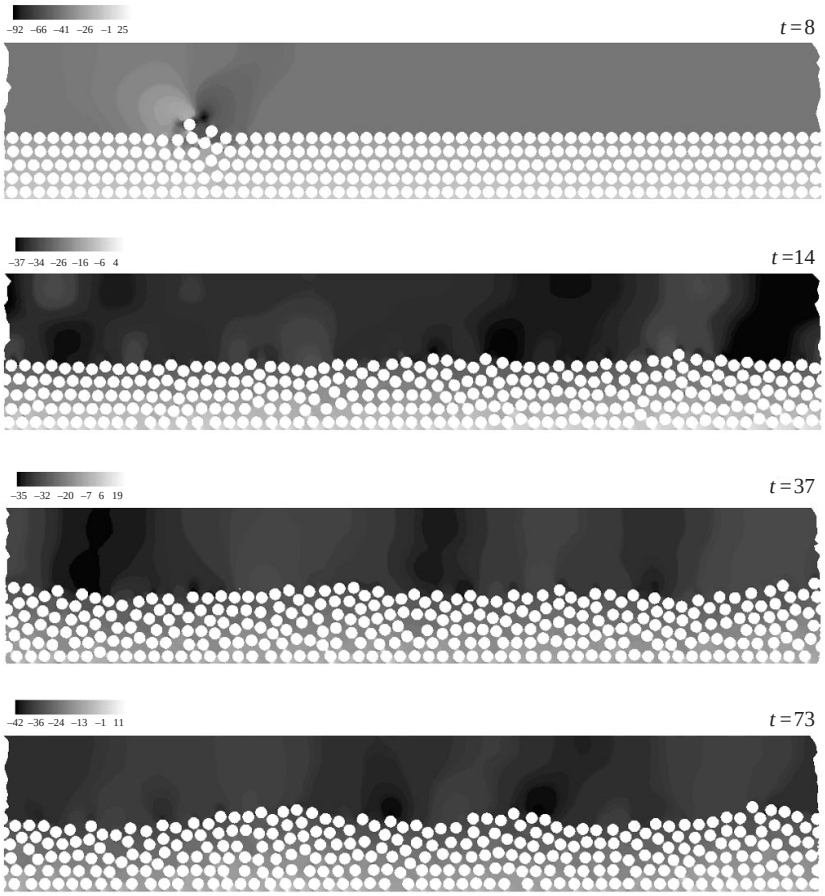

FIGURE 5. Fluidization of 300 particles ($R_G = 981,\ R = 120$). The flow is from left to right. The bed height rises slightly.

Since

$$\epsilon_{\max} = 1 - \phi_{\min} = 1 - \frac{\pi(Nd/l)}{4(W/d)}, \tag{6}$$

it follows that

$$R_G = f\left(R, \epsilon, \epsilon_{\max}, \frac{W}{d}\right), \tag{7}$$

where $\epsilon_{\max}$ is the maximum possible fluid fraction in the channel and $\phi_{\min}$ is the corresponding value of the minimum particle fraction. The parameter ρ_p/ρ_f arises only in the particle acceleration terms in the governing equations (4). At steady state the average acceleration of the particles is zero. Hence ρ_p/ρ_f is not included as a parameter in (5)–(7). However, the effect of ρ_p/ρ_f can be important in characterizing the transient and the 'mixing' behaviour of the mixture. In our multi-particle simulations, W/d and Nd/l (or $\epsilon_{\max}$) are fixed. The gravity Reynolds number R_G is therefore a function of R and ϵ.

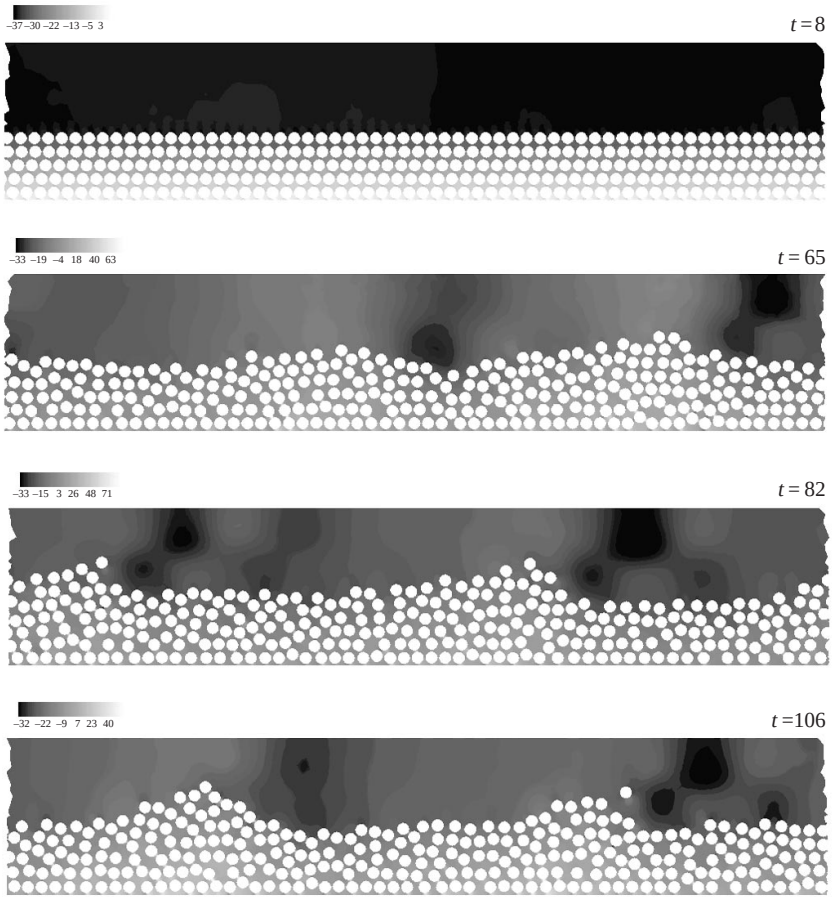

FIGURE 6. Fluidization of 300 particles ($R_G = 981,\ R = 180$). The bed has eroded more ($t = 106$ s).

3. Results

3.1. *Numerical simulation of lift-off*

The gravity Reynolds number, R_G, is varied by changing the viscosity of the suspending fluid. For the given choice of parameters, $R_G = 9.81/\eta^2$. At a given value of R_G, the shear Reynolds number R is varied by changing the applied pressure gradient $\bar{p}$. CJ reported simulations with $\eta = 1$ P and 0.2 P. In this paper we perform simulations with $\eta = 0.1$ P and 0.05 P. The primary objective is to obtain more data to develop a correlation for lift.

Figure 4 shows the contour plot of the axial velocity for a typical simulation. Snapshots of the pressure distribution for several cases are shown in figures 5–17. Light shades indicate high values of pressure. The particles are initially placed in a closely packed ordered configuration. At early times the pressure has vertical stratification. From these figures we observe that the top layer of the particles 'disturbs' the flow, thus giving rise to regions of high pressure at the front of each particle and low pressure at the back. This disturbance causes a horizontal wave of the dynamic pressure with a periodic length of few particle diameters in the clear fluid region. The fluid–mixture interface forms troughs and crests corresponding to the pressure wave.

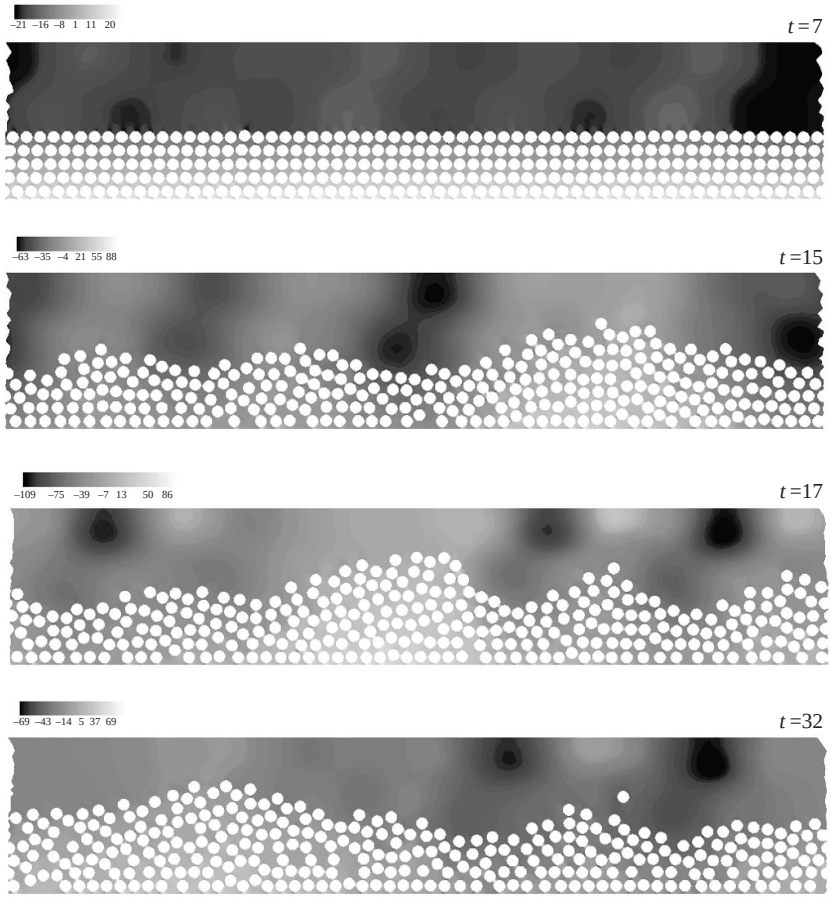

FIGURE 7. Fluidization of 300 particles ($R_G = 981,\ R = 300$).

These interfacial waves, which are more prominent at higher shear Reynolds numbers, grow in amplitude resulting in bed erosion. Similar observation was reported by CJ.

Figures 4, 10, 11, 16 and 17 exhibit intense vortex motion in the early transients prior to the final bed expansion. Drag forces are important in the transients but the final bed height is determined by balance of buoyant weight and lift.

Figures 18 and 19 shows the average height $\bar{H}$ of the particle bed for the additional cases reported here. We observe that the increase in $\bar{H}$ is monotonic at lower shear Reynolds numbers. The graph of $\bar{H}$ eventually levels off to a constant steady value. At higher shear Reynolds numbers ($R > 300$) there is an overshoot in the bed height during the transient. At sufficiently high shear Reynolds numbers the overshoot is large enough for the particles to occupy the entire channel during the transient (figures 4, 10, 11, 12–17). The bed finally settles to the steady equilibrium height. The amplitude of the waves formed on the fluid–mixture interface increases during the transient to cause bed erosion. At high shear Reynolds numbers the interfacial waves are more unstable resulting in the waves reaching the upper wall of the channel. The average lift on the particles increases with the particle fraction. At the peak height the average lift on the particles is not sufficient. Hence, they settle to a lower equilibrium height with larger particle fraction resulting in greater average lift.

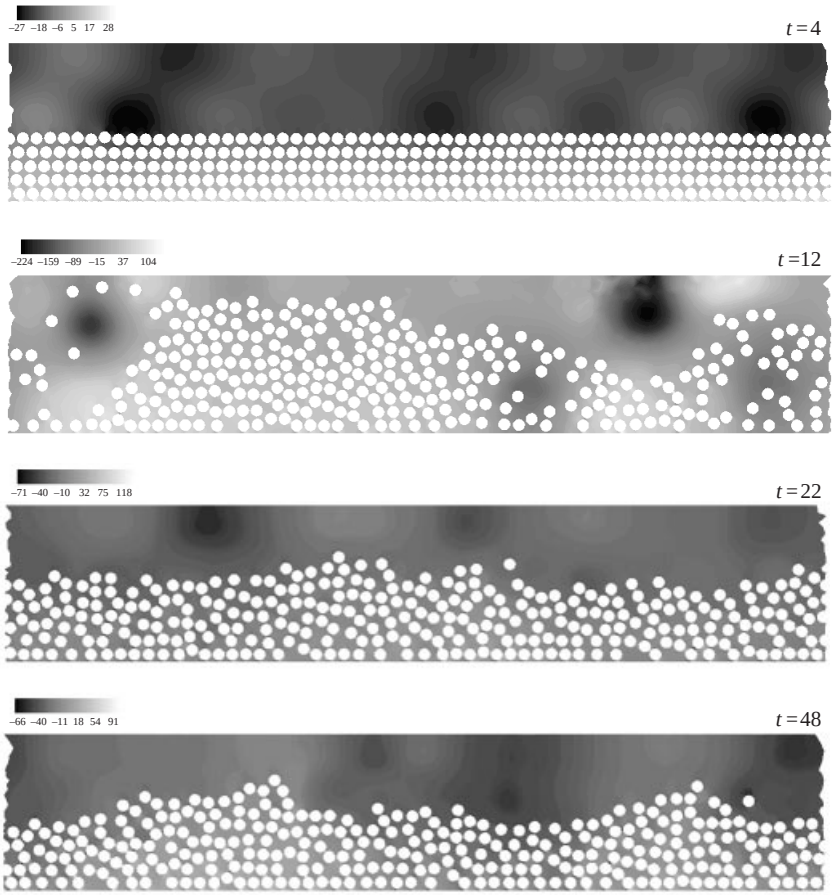

FIGURE 8. Fluidization of 300 particles ($R_G = 981,\ R = 420$). The bed height increases with R.

Another interpretation is that the shear at the top wall drives the particles near it towards the channel centre thus reducing the average height (CJ).

Figures 5–17 show that in the final state there are internal pressure waves which propagate horizontally. The pressure waves cause compression and rarefaction in the particle bed when the average equilibrium height is large. The waves of horizontal stratification of the particle fraction propagate with the pressure wave. Similar observations were reported by CJ. At lower values of the equilibrium height, the particles are close to one another and cannot be pushed together without driving some vertically upwards. This results in waves on the fluid–mixture interface, similar to those formed during the initial transient, which propagate with the pressure waves. In contrast to the waves formed during the transient phase, the waves in the final state are smaller in amplitude and do not grow.

Wave formation in sediment transport by water has been observed before in various scenarios (Kennedy 1969; Graf 1971; Bagnold 1973). Wind-generated ripples and dunes were discussed by Bagnold (1941). Wave-like motion in pneumatic transport was studied by Wen & Simons (1959) and Tomita, Jotaki & Hayashi (1981) among others. Wave-like slugs, which resemble solitary waves in an open channel, are observed in pneumatic transport (Wen & Simons 1959). Similar plugs are observed during the transient phase in our simulations (figure 8, $t = 12$ s). The plug is unstable

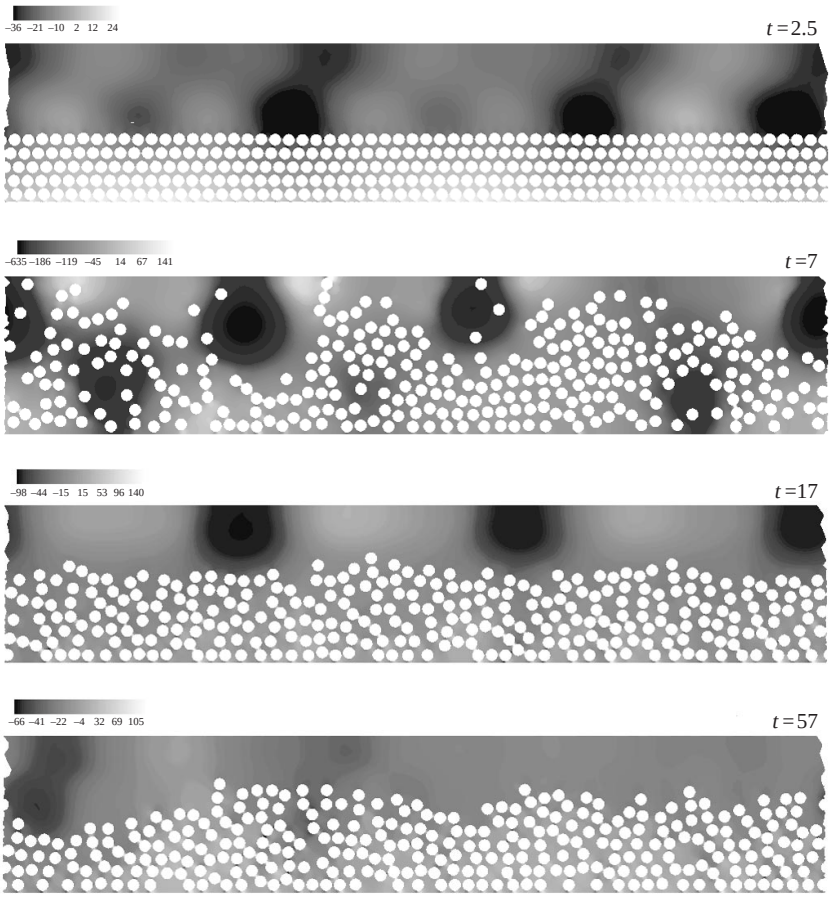

FIGURE 9. Fluidization of 300 particles ($R_G = 981,\ R = 600$).

and eventually breaks to settle to the final equilibrium height. Three different modes of transport of particles in water have been observed (Abbott & Francis 1977) – rolling, saltation and suspension. Kern, Perkins & Wyant (1959) reported similar modes for proppant transport in fractured reservoirs. All these modes are observed in our simulations. We observe rolling when the bed is not eroded at low Reynolds numbers. Waves are observed during the initial transient and the final steady state at relatively low equilibrium heights (figures 5–17). The suspension of particles without interfacial waves is observed when the particle fraction at steady state is low (figures 10 and 11).

Previous investigations of the fluidization of many particles by shear have focused on the creeping flow limit (see Morris & Brady 1998 and references therein) and on particle dispersion due to turbulence (Bagnold 1941; Graf 1971). In the creeping flow limit the hydrodynamic interaction between the particles tends to disperse them into regions of lower concentrations. This shear-induced diffusivity balances gravitational settling. In turbulent flows, the solids are suspended against gravity by random eddy currents. The results of our simulations are valid for a range of Reynolds numbers.

The maximum value of R in our simulations is 2400 (figure 17). We can also define a Reynolds number $R_W = \rho_f V_{\max} W/\eta$ based on the channel width, where $V_{\max}$ is the maximum velocity in the channel. For the case depicted in figure 17, $R_W = 86\,400$ if $V_{\max}$ is the maximum velocity in the absence of the particles whereas $R_W = 14\,640$

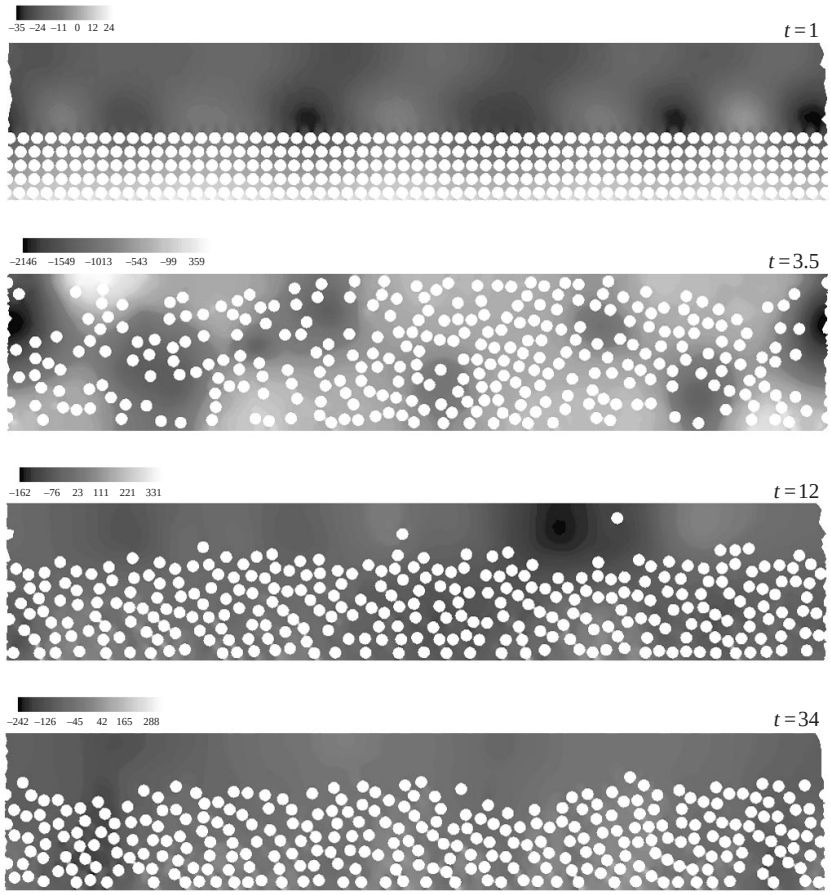

FIGURE 10. Fluidization of 300 particles ($R_G = 981,\ R = 1200$). The bed rises at $t = 3.5$ s to the top wall. The bed settles to its final steady equilibrium height. Interfacial waves corresponding to the pressure waves at the final state are not significant since the particle fraction is not very high.

for the same case if $V_{\max}$ is obtained from the simulation. The length scale (channel width) used in defining the Reynolds number R_W may be inappropriate. A more appropriate length scale could be the spacing between the particles in the particle bed or the height of the clear fluid region in the upper part of the channel. Using height of the clear fluid region as the length scale, the calculated Reynolds number for the case in figure 17 is 5490. One might expect results, unlike those from our simulations, with turbulent flow features at these Reynolds numbers. The effect of large particles on fluid turbulence at high particle fractions is not well understood. Particles can enhance or suppress turbulence. It has been suggested that large particles can cause enhancement of turbulence due to wake shedding (Hetsroni 1989). In our simulations wake shedding is not significant (figures 5–17). The difference between the average fluid and particle velocities (slip velocity) is very small (also see CJ). The presence of the particles increases the resistance to the flow; this increased resistance can be interpreted as an increase of apparent viscosity. This may lead to turbulence suppression in cases such as in our simulations where the particle fraction is relatively high. However, the upper part of the channel is often free from particles and not

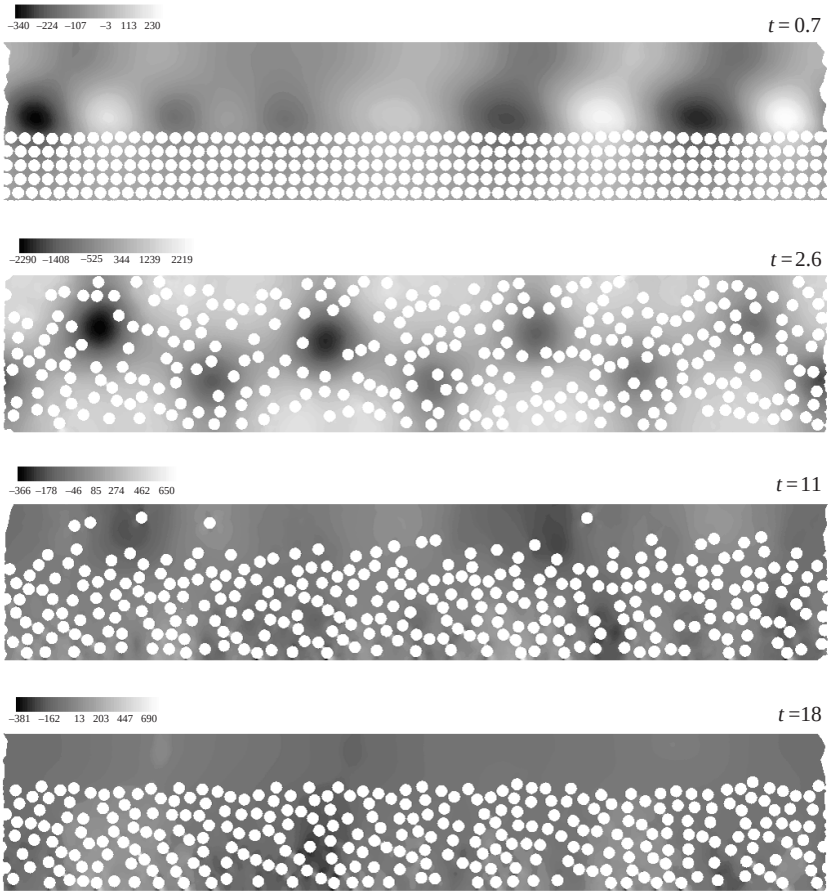

FIGURE 11. Fluidization of 300 particles ($R_G = 981,\ R = 1800$). Interfacial waves at the final state are not significant.

subjected to turbulence suppression. The lack of turbulence there may be an effect of two-dimensionality.

3.2. *Correlation for lift-off*

We obtain a correlation for the average equilibrium height of the particles based on the data from our simulations and those reported by CJ. Since W/d and Nd/l (or $\epsilon_{\max}$ are fixed, the gravity Reynolds number R_G is a function of R and ϵ.

The effective weight of a particle in a suspension is

$$(\pi d^2/4)(\rho_p - \rho_c)g = \epsilon(\pi d^2/4)(\rho_p - \rho_f)g$$

(Foscolo & Gibilaro 1984; Joseph 1990), where ρ_c is the effective or composite density of the fluid–particle mixture. Consequently, the net buoyant weight (or lift) L_s on a particle in a suspension is given by

$$L_s = \epsilon L = \epsilon(\pi d^2/4)(\rho_s - \rho_f)g. \tag{8}$$

We therefore plot ϵR_G vs. R in figure 20 at different values of fluid viscosities. At a given viscosity the value of R_G is a constant in our simulations. The fluid fraction or the equilibrium height of the particle bed increases as the shear Reynolds number

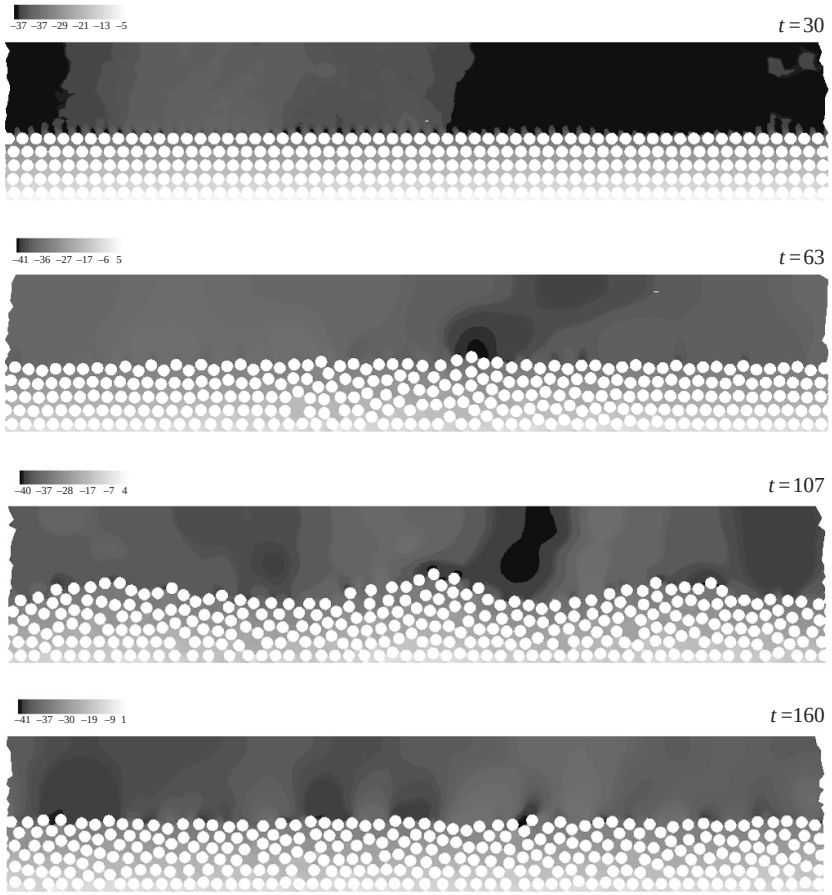

FIGURE 12. Fluidization of 300 particles ($R_G = 3924,\ R = 240$).

is increased. Heavier particles are lifted to a smaller equilibrium height at the same shear Reynolds number. We observe that the data at each viscosity (or R_G) can be represented by a power law equation of the form $\epsilon R_G = cR^m$, where the values of c and m are given in the figure. The value of c varies significantly with respect to R_G whereas the value of m does not show large variation. Figure 21 shows the plot of c vs. R_G on a logarithmic scale. The functional dependence of c on R_G is represented in terms of a power law equation. Combining this result with that in figure 20 we can arrive at a correlation for R_G as a function of R and ϵ. In figure 22 we reduce all the data points to a single curve. The prefactor in the expression for c is changed from 0.368 in figure 21 to 0.4119 in figure 22 for better agreement between the data and the correlation. The average value of the exponent m is also obtained from the curve fit for all the data points. We obtain the following correlation for R_G as a function of R and ϵ:

$$R_G = 3.27 \times 10^{-4}\epsilon^{-9.05}R^{1.249}$$
$$\Rightarrow \epsilon R_G = 3.27 \times 10^{-4}\epsilon^{-8.05}R^{1.249}. \tag{9}$$

The data from which the correlation is derived had the following range of parameters: ϵ between 0.29 and 0.69, R_G ranging from 9.81 to 3924 and R ranging from 5.4 to

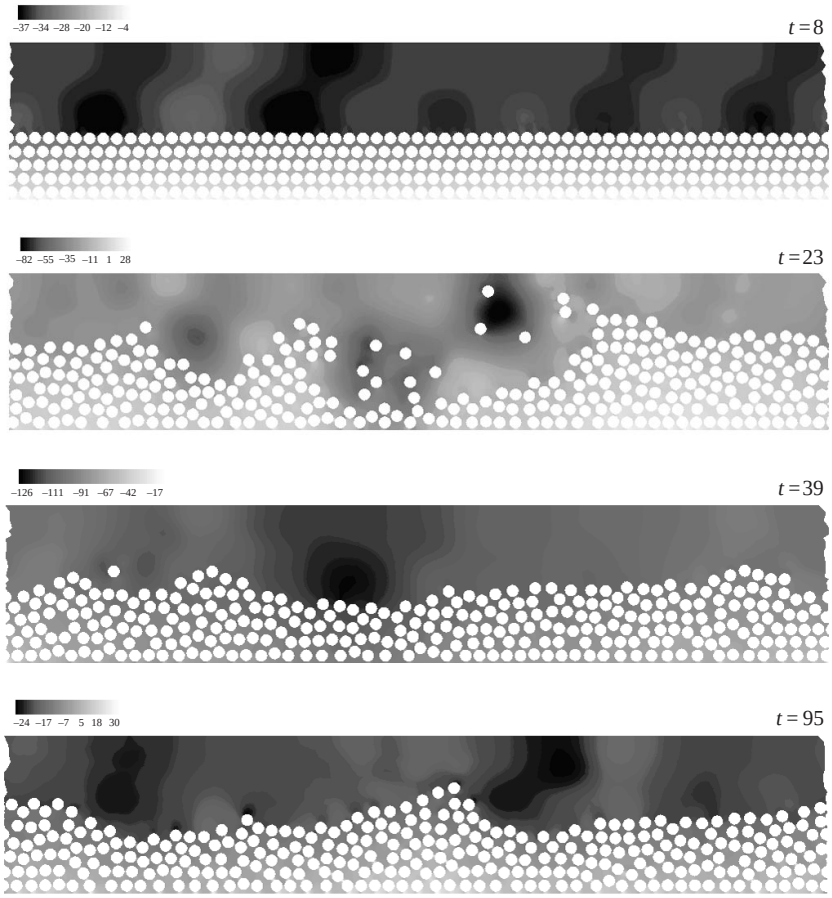

FIGURE 13. Fluidization of 300 particles ($R_G = 3924,\ R = 480$).

2400. It is well-known that particles sedimenting in a suspension experience greater drag at higher particle fractions. Similar behaviour is observed for the hydrodynamic lift force on particles in a suspension (9).

The ratio $2\bar{H}/W$ denotes the fraction of the channel width occupied by the fluid–particle mixture. The correlation can be rewritten in terms of this parameter as

$$R_G = 3.27 \times 10^{-4} \left(\frac{(2\bar{H}/W) - \phi_{\min}}{2\bar{H}/W} \right)^{-9.05} R^{1.249}. \tag{10}$$

The correlation in dimensional form is

$$\bar{p} = 1234.88 \left(1 - \frac{N\pi d^2}{8\bar{H}l} \right)^{7.25} \frac{\rho_f g^{0.8} \left(\rho_p/\rho_f - 1 \right)^{0.8} d^{0.4} v^{0.4}}{W}, \tag{11}$$

where v is the kinematic viscosity of the fluid. The effect of W/d and $\epsilon_{\max}$ on the correlation is not investigated.

The lift-off correlation above is valid for the average behaviour of the suspension in a channel. It accounts for the effect of the Reynolds number on the lift-off of many particles. A similar correlation may also be developed based on the experimental data.

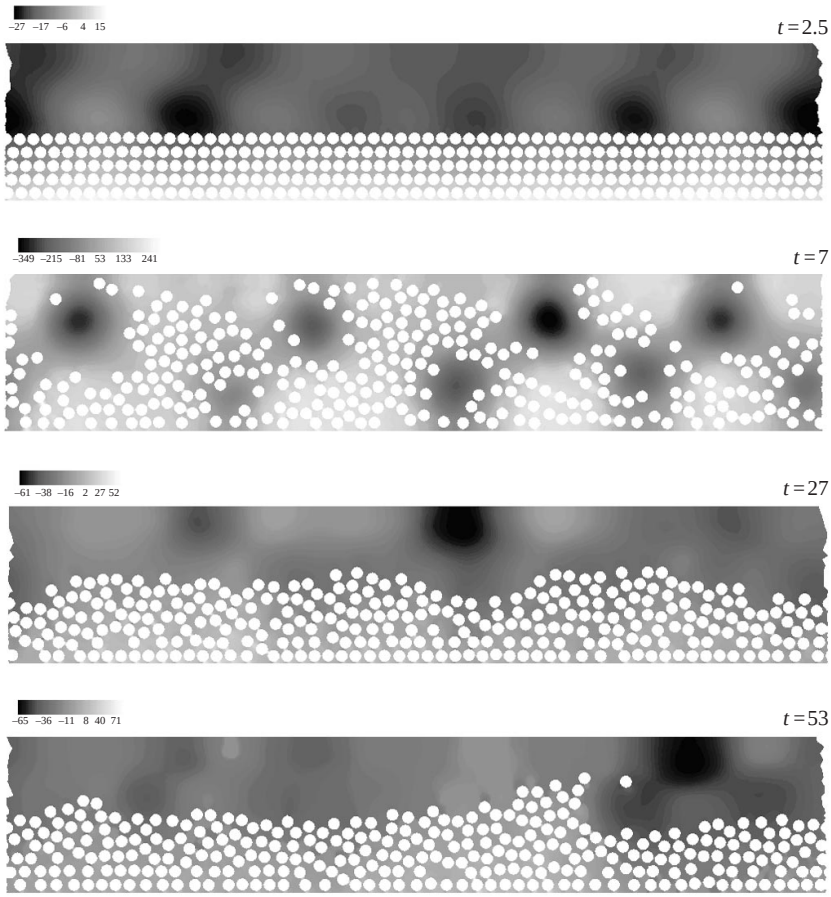

FIGURE 14. Fluidization of 300 particles ($R_G = 3924,\ R = 960$).

The correlation can be used to estimate the critical Reynolds number for lift-off of suspensions in a channel (for the given values of W/d and $\epsilon_{\max}$). Let $2\bar{H}_o$ be the initial height of the closely packed particle bed. Equation (10) implies

$$\frac{(2\bar{H}/W) - \phi_{\min}}{2\bar{H}/W} = \left(\frac{3.27 \times 10^{-4} R^{1.249}}{R_G}\right)^{1/9.05} \stackrel{\text{def}}{=} C. \tag{12}$$

It follows that

$$\frac{2\bar{H}}{W} = \frac{\phi_{\min}}{1 - C}.$$

For fluidization, we have $\bar{H} \geqslant \bar{H}_o$ where the equality represents the critical condition for lift-off. We also have

$$\phi_{\max} = \frac{\pi d^2 N/4}{2\bar{H}_o l}, \tag{13}$$

where $\phi_{\max}$ is the particle fraction in the initial closely packed configuration and $\phi_{\min}$ is given in (6) as

$$\phi_{\min} = \frac{\pi d^2 N/4}{W l} = \frac{2\bar{H}_o}{W}\phi_{\max}. \tag{14}$$

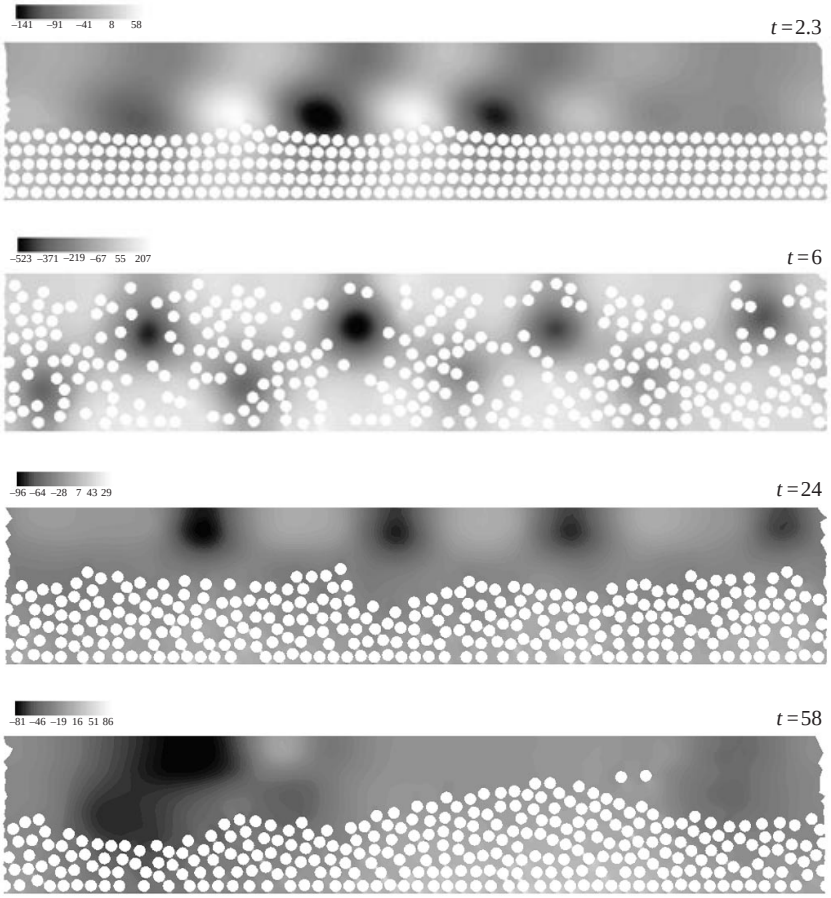

FIGURE 15. Fluidization of 300 particles ($R_G = 3924,\ R = 1200$).

The condition for lift-off is then given by

$$\frac{2\bar{H}}{W} = \frac{\phi_{\min}}{1-C} \geqslant \frac{2\bar{H}_o}{W}.$$

After replacing $\phi_{\min}$ with $\phi_{\max}$, using (14), we find

$$\frac{2\bar{H}_o}{W}\frac{\phi_{\max}}{1-C} \geqslant \frac{2\bar{H}_o}{W}.$$

Hence

$$C \geqslant 1 - \phi_{\max}. \tag{15}$$

Combining now (12) and (15) we get

$$R \geqslant \left(\frac{R_G}{3.27 \times 10^{-4}}[1-\phi_{\max}]^{9.05}\right)^{1/1.249},$$

where equality represents the critical shear Reynolds number R_{cr} for the lift-off of particles from the bed.

The correlation can also be used to estimate the smallest shear Reynolds number R_{cf} at which the particles would occupy the entire channel width at steady state

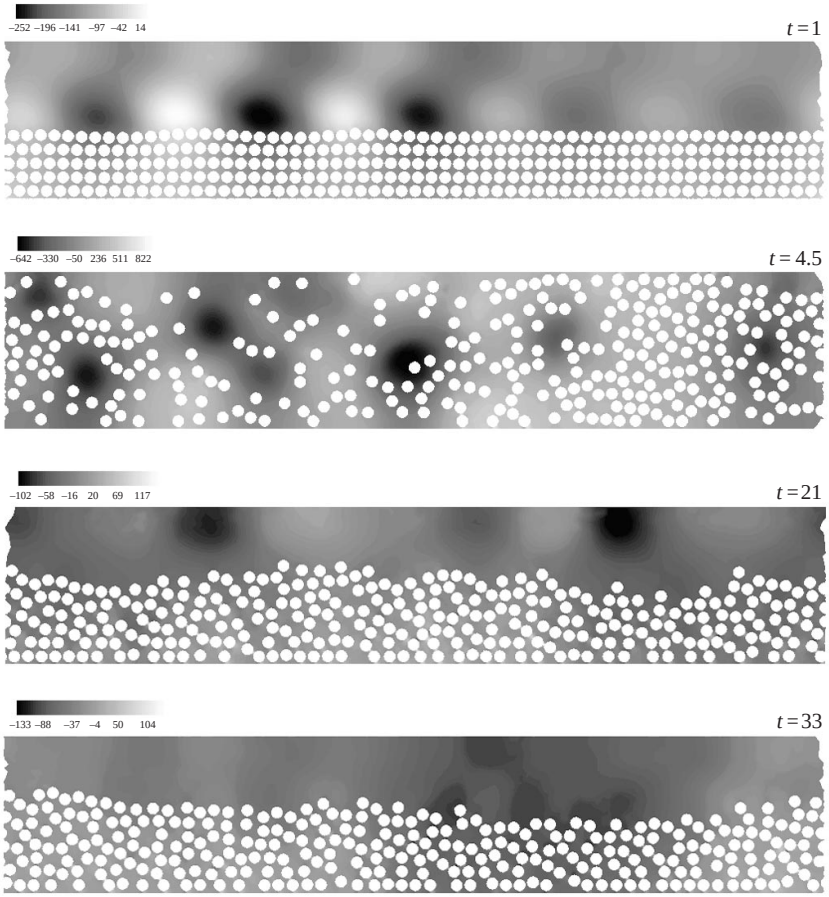

FIGURE 16. Fluidization of 300 particles ($R_G = 3924,\ R = 1680$).

($2\bar{H} = W$). Following steps similar to those in (15) we get

$$R_{cf} = \left(\frac{R_G}{3.27 \times 10^{-4}} [1 - \phi_{\min}]^{9.05} \right)^{1/1.249}. \tag{16}$$

It cannot be predicted with certainty that the particles will occupy the entire channel width at this Reynolds number. The effect of the upper wall may prevent such a possibility. The estimated value of R_{cf} may also be within the turbulent regime.

Patankar *et al.* (2001) obtained a correlation for the critical condition for lift-off of a single circular particle in a plane Poiseuille flow of a Newtonian fluid. They assumed a surface roughness of $0.001d$ and defined the critical condition as the minimum shear Reynolds number required to lift a particle to an equilibrium height greater than $0.501d$. Their correlation is given by

$$R_{cr,1} = (R_G/2.36)^{1.39}, \tag{17}$$

where $R_{cr,1}$ is the critical shear Reynolds number for lift-off of a single particle. Equation (17) is valid for $W/d \geqslant 12$.

Table 1 compares R_{cr} and $R_{cr,1}$ for the values of R_G listed in figure 20. In our simulations we had $\phi_{\max} = 0.71$ and $\phi_{\min} = 0.31$. The values of R_{cf} are also listed.

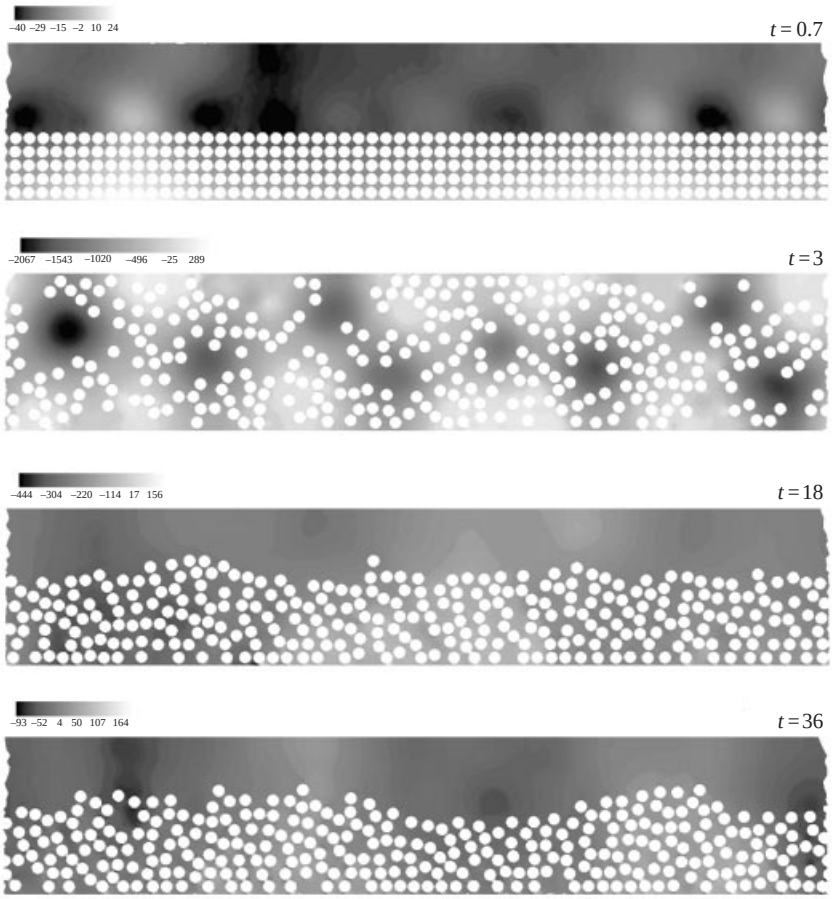

FIGURE 17. Fluidization of 300 particles ($R_G = 3924,\ R = 2400$).

The shear Reynolds numbers in our computations are between R_{cr} and R_{cf} at all values of R_G. Due to the computational cost, many particle simulations were not performed to confirm the value of R_{cr} estimated from the correlation. The average bed height did not increase after a long computation when the shear Reynolds number was less than R_{cr} for some cases we tested. Table 1 shows that the critical shear Reynolds number for lift-off of a single particle is greater than that for many particles at the same value of R_G. This is similar to the fluidization of particles by drag where the critical velocity for fluidization of a single particle is more than that for many particles.

The previous investigation by Morris & Brady (1998) addresses the problem of lift-off of many particles in the creeping flow limit. They considered the balance between gravitational settling and Fickian diffusion of particles. The diffusivity in their simulations was the shear-induced diffusivity driven by hydrodynamic interactions between the particles. In their analysis the average height of the particle bed depends on a dimensionless parameter B characterizing the relative strength of buoyancy to shearing. It can be verified that their parameter $B \sim O(R_G W/Rd)$. Therefore, in the creeping flow limit, $R_G/R = f(\epsilon, Nd/l, W/d)$ instead of the general form at finite Reynolds numbers in (5). At finite Reynolds numbers, inertia plays a role in the balance of the buoyant weight and the hydrodynamic lift on the particles.

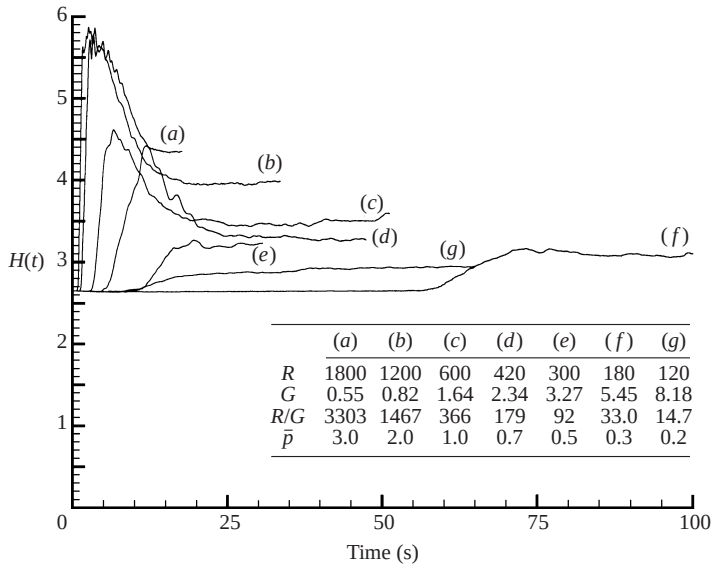

	(*a*)	(*b*)	(*c*)	(*d*)	(*e*)	(*f*)	(*g*)
R	1800	1200	600	420	300	180	120
G	0.55	0.82	1.64	2.34	3.27	5.45	8.18
R/G	3303	1467	366	179	92	33.0	14.7
$\bar{p}$	3.0	2.0	1.0	0.7	0.5	0.3	0.2

FIGURE 18. Rise curves for the average height of 300 circular particles fluidized by lift ($\eta = 0.1P$, $R = 600\bar{p}$, $R_G = 981$, $\bar{p}$ is in dyn cm^{-2}). Notice the overshoot at early times. The final bed height is an increasing function of $\bar{p}$. The bed is at steady state when the rise curve levels off. The time to steady state is longer when the Reynolds number is smaller.

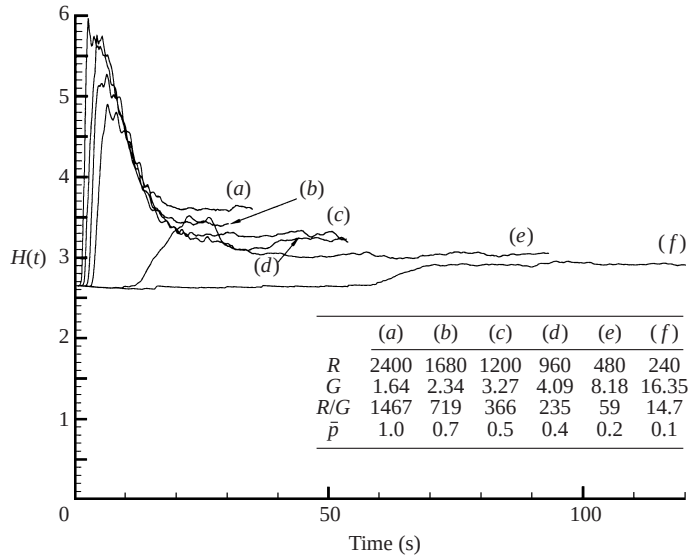

	(*a*)	(*b*)	(*c*)	(*d*)	(*e*)	(*f*)
R	2400	1680	1200	960	480	240
G	1.64	2.34	3.27	4.09	8.18	16.35
R/G	1467	719	366	235	59	14.7
$\bar{p}$	1.0	0.7	0.5	0.4	0.2	0.1

FIGURE 19. Rise curves for the average height of 300 circular particles fluidized by lift ($\eta = 0.05P$, $R = 2400\bar{p}$, $R_G = 3924$, $\bar{p}$ is in dyn cm^{-2}).

Models for the drag force on particles in solid–liquid mixtures, which rely on the well-known Richardson–Zaki (1954) correlation, are usually obtained in terms of the single particle drag formula, Reynolds number and the fluid fraction. Reduction of the lift-off correlation in (9) in terms of the single-particle lift formula is not straightforward. This is because more than one equilibrium position is possible for a single particle in a channel (CJ; Patankar *et al.* 2001). Patankar *et al.* (2001) have

R_G	R_{cr}	$R_{cr,1}$	R_{cf}
9.81	0.461	2.787	256.62
245.25	6.061	28.24	3377.06
981	18.39	76.56	10246.4
3924	55.80	207.56	31088.9

TABLE 1. Comparison between the critical Reynolds numbers for lift-off of many particles and a single particle at different values of R_G. The smallest shear Reynolds numbers at which the particles would occupy the entire channel width at steady state are also listed.

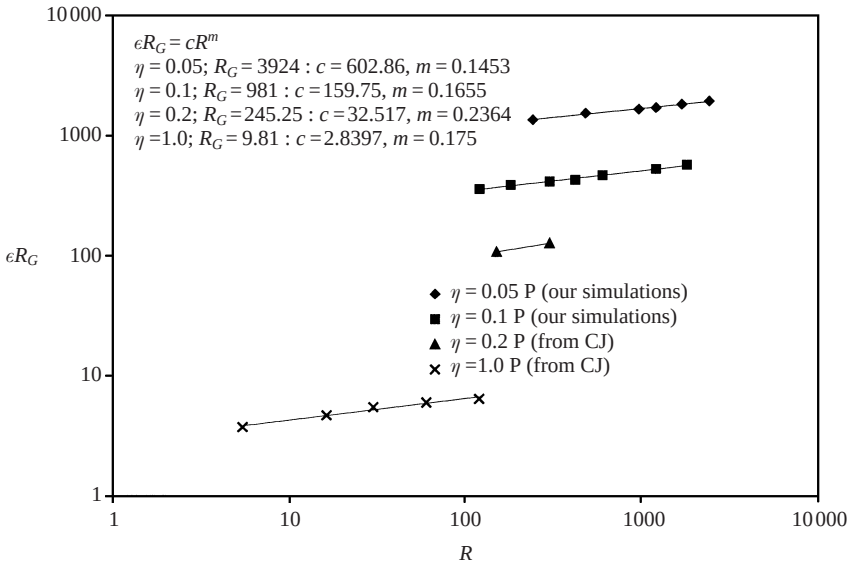

FIGURE 20. A plot of ϵR_G *vs.* the shear Reynolds number R on a logarithmic scale for 300 particles in plane Poiseuille flows of Newtonian fluids at different values of fluid viscosities (or R_G).

identified this as a double-turning-point solution. We have not observed multiple equilibrium heights of the particle bed in our many-particle simulations.

4. Conclusions

Two-dimensional numerical simulations of the lift-off of 300 circular particles in plane Poiseuille flows of Newtonian fluids have been performed. Lift-off is initiated by the formation of horizontal pressure waves and the corresponding waves at the fluid–mixture interface. At low shear Reynolds numbers, there is a monotonic increase of the average height of the particle bed to the final equilibrium value. At higher shear Reynolds numbers ($R > 300$) there is an overshoot in the bed height, with particles sometimes occupying the entire channel width, during the transient. The bed finally settles to a lower equilibrium height for the cases considered here. In the final state there are internal pressure waves which propagate horizontally. There are corresponding waves in the particle bed. The average fluid fraction of the particle bed increases as the shear Reynolds number is increased. Heavier particles are lifted to a smaller equilibrium height at the same Reynolds number.

A correlation for the lift-off of many particles in two dimensions is obtained from

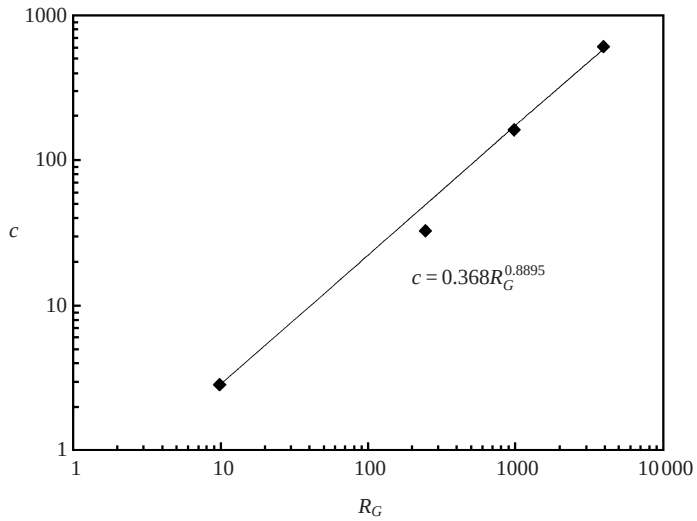

FIGURE 21. A plot of c *vs.* R_G on a logarithmic scale.

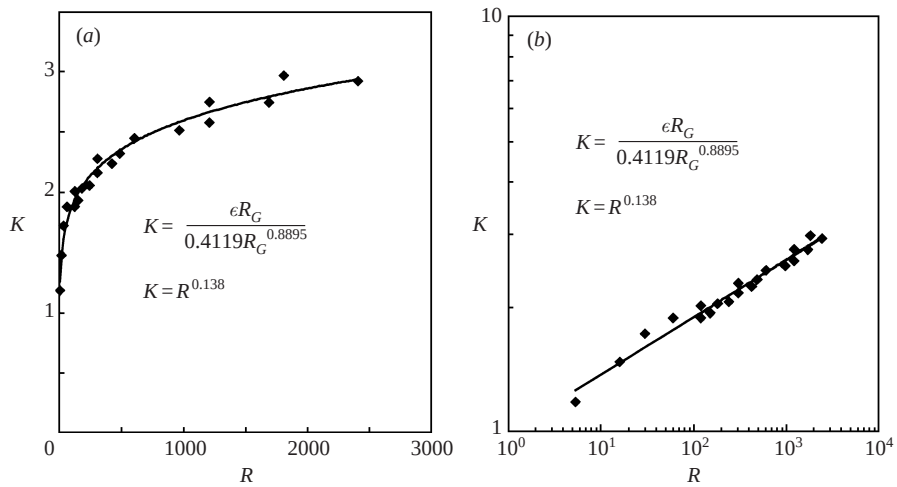

FIGURE 22. Correlation for lift-off from numerical simulations of 300 circular particles in plane Poiseuille flows of Newtonian fluids ($W/d = 12$). (*a*) Regular scale, (*b*) logarithmic scale.

the numerical data modelling procedures and will be used in getting correlations that we think will emerge from three-dimensional simulations at present underway. The correlation is used to estimate the critical shear Reynolds number for lift-off of many particles and the smallest shear Reynolds number at which the particles would occupy the entire channel width at steady state. The critical shear Reynolds number for lift-off of a single particle is greater than that for many particles at the same value of R_G. This is similar to the fluidization of particles by drag where the critical velocity for fluidization of a single particle is more than that for many particles.

This work was partially supported by the National Science Foundation KDI/New Computational Challenge grant (NSF/CTS-98-73236), by the US Army, Mathematics,

by the DOE, Department of Basic Energy Sciences, by a grant from the Schlumberger foundation and from Stimlab Inc. and by the Minnesota Supercomputer Institute.

REFERENCES

Abbott, J. & Francis, J. R. D. 1977 Saltation and suspension trajectories of solid grains in a water stream. *Phil. Trans. R. Soc. Lond.* A **284**, 225–254.

Bagnold, R. A. 1941 *The Physics of Blown Sands and Desert Dunes*. Methuen, London.

Bagnold, R. A. 1973 The nature of saltation and of 'bed-load' transport in water. *Proc. R. Soc. Lond.* A **332**, 473–504.

Choi, H. G. 2000 Splitting method for the combined formulation of fluid-particle problem. *Comput. Meth. Appl. Mech. Engng* **190**, 1367–1378.

Choi, H. G. & Joseph, D. D. 2001 Fluidization by lift of 300 circular particles in plane Poiseuille flow by direct numerical simulation. *J. Fluid Mech.* **438**, 101–128 (referred to herein as CJ).

Chorin, A. J. 1968 Numerical solution of the Navier–Stokes equations. *Math. Comput.* **22**, 745–762.

Foscolo, P. V. & Gibilaro, L. G. 1984 A fully predictive criterion for transition between particulate and aggregate fluidization. *Chem. Engng Sci.* **39**, 1667–1675.

Graf, W. H. 1971 *Hydraulics of Sediment Transport*. McGraw-Hill.

Hetsroni, G. 1989 Particle-turbulence interaction. *Intl J. Multiphase Flow* **15**, 735–746.

Hu, H. H. 1996 Direct simulation of flows of solid-liquid mixtures. *Intl J. Multiphase Flow* **22**, 335–352.

Hu, H. H., Joseph, D. D. & Crochet, M. J. 1992 Direct numerical simulation of fluid particle motions. *Theoret. Comput. Fluid Dyn.* **3**, 285–306.

Hu, H. H. & Patankar, N. A. 2001 Simulation of particulate flows in Newtonian and viscoelastic fluids. *Intl J. Multiphase Flow* (to appear).

Hu, H. H., Patankar, N. A. & Zhu, M.-Y. 2001 Direct numerical simulations of fluid-solid systems using the Arbitrary-Lagrangian-Eulerian technique. *J. Comput. Phys.* **169**, 427–462.

Joseph, D. D. 1990 Generalization of the Foscolo-Gibilaro analysis of dynamic waves. *Chem. Engng Sci.* **45**, 411–414.

Joseph, D. D. 2001 Interrogations of direct numerical simulation of solid-liquid flow. http://www.acm.umn.edu/people/faculty/joseph/interogation/html

Kennedy, J. F. 1969 The formation of sediment ripples, dunes and antidunes. *Ann. Rev. Fluid Mech.* **1**, 147–168.

Kern, L. R., Perkins, T. K. & Wyant, R. E. 1959 The mechanics of sand movement in fracturing. *Petrol. Trans. AIME* **216**, 403–405.

Ko, T., Patankar, N. A. & Joseph, D. D. 2001 A note on the lift-off of a single particle in viscoelastic fluids. *Phys. Fluids* (submitted).

Morris, J. F. & Brady, J. F. 1998 Pressure-driven flow of a suspension: buoyancy effects. *Intl J. Multiphase Flow* **24**, 105–130.

Patankar, N. A., Huang, P. Y., Ko, T. & Joseph, D. D. 2001 Lift-off of a single particle in Newtonian and viscoelastic fluids by direct numerical simulation. *J. Fluid Mech.* **438**, 67–100.

Richardson, J. F. & Zaki, W. N. 1954 Sedimentation and fluidization: Part I. *Trans. Inst. Chem. Engrs* **32**, 35–53.

Tomita, Y., Jotaki, T. & Hayashi, H. 1981 Wavelike motion of particulate slugs in a horizontal pneumatic pipeline. *Intl J. Multiphase Flow* **7**, 151–166.

Wen, C. Y. & Simons, H. P. 1959 Flow characteristics in horizontal fluidized solids transport. *AIChE J.* **5**, 263–267.